This is a preprint of a paper intended for publication in a journal or proceedings. Since changes may be made before publication, this preprint is made available with the understanding that it will not be cited or reproduced without the permission of the author.

UCRL - 77197
PREPRINT
Conf-750852--3

LAWRENCE LIVERMORE LABORATORY
University of California/Livermore, California

HIGH ENERGY GLASS LASERS

James A. Glaze

August 15, 1975

MASTER

NOTICE
This report was prepared as an account of work sponsored by the United States Government. Neither the United States nor the United States Energy Research and Development Administration, nor any of their employees, nor any of their contractors, subcontractors, or their employees, makes any warranty, express or implied, or assumes any legal liability or responsibility for the accuracy, completeness or usefulness of any information, apparatus, product or process disclosed, or represents that its use would not infringe privately owned rights.

This Paper was Prepared for Submission to the
PROCEEDINGS of the 19th Annual Technical Symposium of the
Society of Photo-Optical Instrumentation Engineers
August 18-22, 1975, San Diego, California

DISTRIBUTION OF THIS DOCUMENT UNLIMITED

HIGH ENERGY GLASS LASERS*

James A. Glaze
Laser Fusion Division, Lawrence Livermore Laboratory
Livermore, California 94550

Introduction

A number of laboratories throughout the world are actively pursuing the development of pulsed high power Nd:glass lasers for use in their laser fusion and laser plasma interaction studies programs. Perhaps the most ambitious programs in this field have been undertaken by the Lawrence Livermore Laboratory where several irradiation facilities are in operation and where the 4-arm ARGUS and 20-arm SHIVA lasers are currently under construction. These systems are designed to provide the energy, power and wavefront uniformity required to spherically implode nuclear fuel targets such as the deuterium-tritium (DT) solid sphere, in an effort to achieve thermonuclear fusion through inertial confinement.[1]

The requirements on the optical performance of fusion lasers are staggering. Targets as small as 100 microns in diameter must be uniformly irradiated with multiple beams each delivering between 100 and 1000 joules of energy. This energy must be delivered in a single, time-tailored pulse whose peak power exceeds one terawatt. To achieve the required uniformity and brightness of illumination at this power level, numerous linear and non-linear propagation phenomena must be thoroughly understood and addressed in a pragmatic manner.

To investigate intense pulse propagation phenomena, as well as problems in laser and system design, we have built and have operated a prototype single chain laser called CYCLOPS.[2] This laser employs a 20-cm clear aperture disk amplifier in its final stage and produces a terawatt pulse whose brightness exceeds 10^{18} watts/cm^2-ster. In this paper we summarize the CYCLOPS system and discuss aspects of non-linear propagation phenomena that are currently being addressed.

*This work was performed under the auspices of the U.S. Energy Research and Development Administration.

The CYCLOPS Laser

The CYCLOPS laser chain is shown schematically in Figure 1. The Nd:YAG dye mode-locked oscillator with its optically triggered spark gap switch-out produces a single bandwidth-limited pulse whose duration and energy are nominally 100 ps and 1.5 mJ respectively. This pulse is amplified by two stages of rod preamplifiers and three stages of disk amplifiers. The basic staging after initial preamplification includes an iteration of multilayer dielectric coated polarizers and pulsed Faraday rotators. These provide both isolation from target reflections and pre-lasing. Approximately 25 dB of backward attenuation is provided for each 10 dB of gain in the forward direction.

The five rod preamplifiers range in clear aperture from 9.5 mm to 25 mm and deliver a nominal 0.2-joule pulse to the first stage of disk amplifiers. A laser prepulse-isolating dye cell having a small signal transmission of 1.5% and a large signal transmission of 50% is positioned after the 9.5-mm preamplifier. This is followed by a spatial filter and an apodizing aperture.

The disk amplifier stages labeled "A", "B" and "C" have clear circular apertures of 36 mm, 85 mm and 200 mm respectively. Each stage consists of 12 elliptical disks mounted at Brewsters' angle. Each "A" and "B" module houses 6 disks and each "C" module 3 disks. The disks are pumped radially by closely coupled linear flashlamps which range in number from 12 to 32 per module for a total of 184 lamps. The combined capacitive energy storage to fire these lamps is 1.6 megajoules. Figure 2 shows the interior portions of a 20-cm aperture C-module. The elliptical disks in this module are nominally 21 cm X 40 cm X 3 cm in size with a surface flatness of about 1/8 λ at 6328Å and a doping concentrate of 0.02 wt. Nd:O_3. These, like the other disks in the

chain have an absorptive glass edge cladding to suppress parasitic oscillations and reduce fluorescence depumping.

A high energy spatial filter is placed between the B and C amplifier stages. This filter, which is shown in Figure 3, is comprised of an f/10 lens - pinhole combination housed in an evacuated chamber. Chamber pressure is kept below 10^{-5} torr to reduce the possibility of air or material breakdown at the 300 micron diameter diamond pinhole.

A pair of rotatable cylindrical lenses used to correct linear astigmatism are placed after the spatial filter. This pair has a range of about three waves and are adjusted by monitoring the far-field pattern of a cw beam that traverses the same path as that of the pulsed beam.

Figure 4 is a simplified schematic of the laser chain showing typical values of power at each stage. Figure 5 is a photograph of the chain looking backward from a position at the final output stage.

Small Scale Self-Focusing

Beam instability resulting from intensity-induced small-scale self-focusing is, today, the single most limiting factor in achieving increased brightness from the Nd:glass laser. This phenomenon is manifest in the near field by the presence of structured beam filaments whose intensity can exceed the average by several orders of magnitude,[3] and in the far-field by a broadening of the central focused spot. The one-dimensional linearized instability theory of Bespalov and Talanov predicts that small intensity perturbations ΔI superimposed on a uniform plane wave of intensity I_0 exhibit approximately exponential growth.[4] This is written as

$$\Delta I = I_0 \exp\left[\int g_K \, dz\right] \qquad (1)$$

where the small signal gain, g_K is expressed as

$$g_K = K\left(\frac{\gamma I_o(z)}{n} - \frac{K^2}{4k^2}\right)^{1/2} \qquad (2)$$

In these expressions K is the spatial wavenumber of the perturbation, k the light wave number, n the linear index of refraction and γI_o the nonlinear contribution to the index. In a test of this theory, Bliss et.al. have investigated the growth of interference fringes superimposed on a uniform gaussian beam propagating through an unpumped ED-2 rod for several values of K.[5] Figure 6 shows the growth of such fringes, here spaced 2 mm apart on a pulse with a peak intensity of 5 GW/cm^2. In this work qualitative agreement was obtained between experiment and the predictions of Eqs. (1) and (2) when the data was averaged over the temporal profile of the pulse. Excellent agreement was obtained, however, when the linearized theory was modified to include the relationship between the phase and amplitude of the initial interference fringe modulation.

The consequences of beam breakup on the focusing properties of the beam have also been investigated by Bliss.[6] Figure 7 shows the evolution of the far-field energy distribution as the level of beam breakup is increased. This data was obtained by propagating a 1-cm diameter gaussian temporal and spatial beam through an unpumped ED-2 laser rod and focusing through a 500-μradian aperture. The ordinate gives the ratio of the energy density as a function of radius passing through the aperture to that in the initial beam. Two effects are observed; 1) the time averaged focal spot is increased in size and 2) the net energy passing through the aperture is decreased.

A third consequence of breakup is shown in Figure 8 where the time resolved transmission of the aperture shows dramatic temporal distortion at peak power of the initially gaussian pulse. This distortion arises because the filamentation is the largest and hence transmission through the aperture the smallest at the pulse peak.[6]

The consequences of uncontrolled small scale beam breakup are revealed in Figure 9 where a near-field photograph of the CYCLOPS beam taken at the output of the final C amplifier is shown. On this shot the beam energy was about 270 joules and power about 1 terawatt (no spatial filter between the B and C amplifier stages). The structure of this beam has been revealed by the placement of four neutral density filters in front of the camera and near beam center. Filament structure is clearly in evidence; intensity variations of 10:1 can be identified although greater variations are expected to be present within the glass medium.

Spatial Filtering

Low-pass spatial filtering is suggested as a means of reducing the rapid growth of beam filaments. Equation 2 predicts that the spatial wavenumber K_m, corresponding to the fastest growing frequency is

$$K_m = k\sqrt{\frac{2\gamma I}{n_0}} \tag{3}$$

For a lens-pinhole filter with a pinhole of radius a, and a focal length f, the cut-off wavenumber, K_{co}, is given as

$$K_{co} = \frac{ka}{f} \tag{4}$$

If we choose a/f such that

$$K_m > K_{co} \gtrsim Nm/D \tag{5}$$

$$N \gtrsim 7$$

where π/D is the fundamental wavenumber of the diffraction limited beam, then high frequency components can be removed without significant harmonic distortion of the whole-beam. In Equation 5 we have somewhat arbitrarily choosen N such that the intensity of an Airy pattern at the pinhole edge is less than 30 dB down from the central maxima.

In practice Equation 5 is easy to satisfy providing aberrations of the whole-beam are small. If, for example, we consider the CYCLOPS f/10 filter at the B-stage where $I \sim 8$ GW/cm^2, $D \sim 5.6$ cm, $f = 100$ cm and $a = 150$ microns, we have that $K_m \sim 120$ cm^{-1}, $K_{co} \sim 9$ cm^{-1} and $\pi/D = 0.6$ cm^{-1}. For a detailed treatment of an amplifier chain such as CYCLOPS, however, the theory as represented by Equation 2 must be modified to account for the variable intensity throughout the chain resulting from gain/loss and beam expansion. This has been done by Simmons et.al.[7] in their design of the CYCLOPS filter. Their results show that the peak of the gain curve moves to lower values of K ($K_m \sim 20$ for above example); however, Equation 5 is still easily satisfied.

Figure 10 shows the dramatic effect that the B-stage spatial filter has on a beam that is badly degraded by small scale filamentation. Here are shown photographs of the near-field before and after transmission through the filter. Also shown are energy density profiles which have been derived from computer reduced microdensitometer traces.[8]

Small scale structure grows at the expense of the main beam. Although the initial power spectrum of the noise is seldom known, the degree of beam breakup and hence the transmission of the filter can be related phenomenologically to the power density and propagation path length through the glass. A convenient, but by no means unique, measure of breakup is afforded by the integrated gain coefficient of Equation 2 evaluated at K_m and at peak intensity

along the axis.[9] This so-called "B" integral can, for a collimated beam propagating along a path length with constant small signal gain, g, be written as

$$B \equiv \frac{k\gamma}{n_o}\int_z I_p(z)dz = \frac{\gamma I_o}{g}\,(G(z)-1) \qquad (6)$$

where G(z) is the net unsaturated power gain. If the transmitted power through the filter, P_t, is now written as a functional of B,

$$P_t = P_i\, F(B) \qquad (7)$$

where P_i is power input to the filter, then maximum transmission will be obtained for $(dP_t/dz)z_c = o$. Using Equations 6 and 7 the condition for maximum transmission becomes

$$gF(B) + \gamma I_o\, G_c\, \frac{\partial F}{\partial B} = o \qquad (8)$$

where $G_c \equiv \exp(gz_c)$ and is called the critical stage gain.[10,11] The gain, G_c, can be related to the B-integral through Equation 8 to obtain B_c, the optimum value of B for the filtered stage. The transmitted power can then be written as

$$P_t = P_o G_c\, F(B_c) = \left[P_o + \frac{gB_c}{k\gamma}\int F(\mu)da\right] F(B_c) \qquad (9)$$

where P_o is the input power to the stage, $F(\mu)$ the spatial profile of the beam and the integral is performed over the area of the aperture (the integral relates the power and intensity). Given F(B), Equation 8 can be solved to obtain G_c and hence B_c.

Figure 11 shows time averaged power transmission curves for the B-stage filter for several pinhole diameters. Of note is the precipitous drop in transmission for values of $B \gtrsim 4$. Simmons[7] has obtained a three

parameter fit to this data to obtain F(B) and has shown by solving Equation 8 that, for an ideal spatial filter the power transmission is optimized for a value of $B_c = 3.9$.

Whole Beam Distortion

Intensity-induced aberrations arising from whole beam self-focusing can give rise to complicated temporal and spatial variations of the phase and intensity in the focal region.[12,6] Geometrical analysis[13] shows that the near-field non-linear phase retardation $\Delta\phi_{NL}$, and concomittant angular deviation of the rays, in the near-field $\delta\theta_{NL}$, can be simply related to the near-field intensity profile F(μ), through the following equations;

$$\Delta\phi_{NL} = \frac{2\pi\gamma}{\lambda} F(\mu) \int I(z)dz \tag{10}$$

$$\delta\theta_{NL} = \frac{\gamma}{n_0} \mid \nabla_\mu F(\mu) \mid \int I(z)dz. \tag{11}$$

In these expressions the integral is evaluated along the axial ray, and μ is the radial coordinate of a ray (normalized to the aperture radius a) in a plane perpendicular to z. Equations 10 and 11 have been derived for a beam that retains its initial intensity profile throughout the propagation path of the amplifier chain. Two conditions must be met for this so-called "constant shape approximation" to be upheld. These conditions are expressed as follows:

$$\frac{\lambda^2 B^2}{8\pi^2 a^2 n_0^2} \mid \nabla_\mu F(\mu) \mid^2 \ll 1 \tag{12}$$

and

$$Z_c \leq \frac{a^2}{B\nabla_\mu^2 F(\mu)} \tag{13}$$

where

$$B \equiv \frac{2\pi\gamma}{\lambda} \int I(z)dz \tag{14}$$

The left side of Equation 12 is simply the lowest order correction to the phase aberration if the constant shape approximation is relaxed. In Equation 13, Z_c is the free space propagation distance for which adjacent rays, whose angular trajectories are given by Equation 11 will intersect. At points of intersection the intensity and phase profile will distort and geometrical optics no longer become applicable. Equations 12 and 13 can both be satisfied for a laser chain design such as CYCLOPS.

Apodization

The simple form of Equations 10 and 11 suggest that aberrations arising from whole beam self-focusing can be reduced by a judicious choice of the function $F(\mu)$. This choice must be made however so that near-field diffraction ripples which can be amplified by self-focusing are minimized and amplifier apertures are effectively filled by the beam for optimum power extraction. Two aperture functions that we have considered are the so-called super-gaussian and the modified-quadratic profiles.[14] These are written as

$$F(\mu) = \exp(-6.91\ \mu^5) \qquad \text{(Super-gaussian)} \qquad (15)$$

$$F(\mu) = 1 - 1.3\ \mu^2 \qquad (0 < \mu < 0.79)$$

$$= 0.3 \exp\left(\frac{\mu - 0.71}{0.124}\right)^2 \qquad (0.79 < \mu < 1.0) \qquad \text{(Modified-quadratic)} \quad (16)$$

For comparison we also consider the Airy disk profile which has been used in early laser designs. This is written as

$$F(\mu) = 4\left\{\frac{J_1(3.81\ \mu)}{3.81\ \mu}\right\}^2 \qquad \text{(Airy Disk)} \qquad (17)$$

In these forms the functions are normalized to unity along the axis and to 10^{-3} at the hard aperture a. Figure 12 shows a plot of these functions;

it is clear from this figure that the Airy disk does a poor job of filling the aperture. It can be shown that the fill factors, defined as

$$2\int_0^1 F(\mu)\mu d\mu \tag{18}$$

are 0.23, 0.41 and 0.41 for the Airy disk, super-gaussian and modified-quadratic respectively.

Figure 13 shows the relative angular variations of the rays with respect to the z-axis at the exit aperture (Equation 11). It is observed that both the Airy disk and the super-gaussian give rise to angular distributions that would be expected to yield rather complex intensity and phase distributions in focal regions where high brightness and spatial uniformity are required for pellet illumination. The modified-quadratic, on the other hand, yields a simple linear variation over a substantial portion of the aperture. In terms of geometrical optics, the rays associated with the quadratic distribution can be brought to a common focus, whereas other shapes yield a complex distribution of foci along the z-axis.

Focusing of the Aberrated Beam

We consider the focal properties of a beam with whole-beam distortion given by Equation 10. In the paraxial approximation the phase, ϕ, can be written as

$$\phi = Z - \frac{r^2}{2f} - BF(\mu) \tag{19}$$

where Z is the axial distance from the lens, r is the radial coordinate and f is the focal length. Some of the near-field focusing properties of Equation 19 can be investigated with geometrical optics.[13] Two aspects of interest when evaluating the focusing properties of an aperture function $F(\mu)$ are: 1) the distance from the focal point of the lens that a ray

crosses the optical axis of the system (this is a measure of the dynamic motion of the focus;) and 2) the distortion of the intensity distribution resulting from the crossing of adjacent ray pairs (first caustic surface).

The focal point shift, ΔZ, is given as

$$\frac{\Delta Z}{(f^{\#})^2} = \frac{4B}{\mu}\frac{dF}{d\mu}\exp(-t/\tau)^2 \qquad (20)$$

where $f^{\#}$ is the F-number of the focusing lens and a temporal gaussian pulse shape is assumed. For the CYCLOPS system operating at a terawatt, B is about 1.5 waves. If, for example, an $f^{\#}/2.5$ focusing lens is used, the peak focal shift for the quadratic aperture is 93 waves; many times the depth of focus! Equation 19 is a valuable aid in determining the best focusing geometry for a target of a given design.

The beam intensity at the position Z measured from the focusing lens is given by

$$(f^{\#})^2\,\frac{F(\mu Z)}{4(ka)^2} = \frac{F(\mu, Z_{exit})}{\left[\frac{kZ}{(f^{\#})^2} - 4kB\frac{d^2F}{d\mu^2}\right]^2} \qquad (21)$$

where $\mu = r/a$ is the normalized coordinate of a ray tube in the exit aperture at position Z_{exit}. In the plane at position Z, the radial coordinate, r', of the ray tube μ is given by

$$\frac{kr'}{f^{\#}} = \frac{\mu}{2}\left[\frac{k(f-Z)}{(f^{\#})^2} - \frac{4kB}{\mu}\frac{dF}{d\mu}\right] \qquad (22)$$

Figure 14 shows near-field intensity profiles of the focused super-gaussian in the plane $kZ/(f^{\#})^2$ = constant for 2.2 waves of whole beam distortion. Since spherical targets are often placed many Rayleigh ranges from the focal

plane in order to obtain normality between the target surface and light vector, the super-gaussian profile would clearly be unacceptable when the uniformity of illumination is important.

The geometrical treatment described above can only provide an estimate of the focusing properties of a beam with intensity induced aberrations. To examine these properties in detail, a diffraction program called ZAX has been developed by Hunt et.al.[15,16] that can be applied beams with quite arbitrary intensity profiles. Figures 15 and 16 for example, compare the focal volume intensity distributions exhibited by diffraction limited plane waves with super-gaussian and modified quadratic near-field intensity profiles, to those same profiles with 1.5 waves of whole-beam distortion. These figures display contours of constant intensity whose spacing is 1 dB in the u, v- plane, where $u = kr/(f^{\#})$ and $v = kz/(f^{\#})^2$. They show that, in the absence of aberrations, both intensity profiles propagate quite well into the far-field region, but only the quadratic remains relatively distortion free in the presence of the aberration. The super-gaussian shows distortions of the type predicted by the geometrical model.

Summary

Terawatt performance in the 0.1 to 1 nanosecond regime from a single aperture represents the state-of-the-art in high power Nd:glass laser technology today. This has been achieved with the CYCLOPS system using 20-cm clear aperture disks in the final power amplifier stage and a spatial filter for control of small scale self-focusing. Aberrations arising from whole beam-self-focusing can seriously degrade beam focusability by introducing intensity and phase nonuniformities in the intermediate field where spherical targets are likely to be placed. This aberration can be reduced,

however, by the use of quadratic apertures which reduce the distortion to that of a simple time dependent movement of the focal plane. Both ray-tracing and full diffraction codes exist which allow rather complete modeling of propagation phenomena that are of interest in the design of large laser chains.

REFERENCES

1. J. Nuckolls, L. Wood, A. Thiessen, and G. Zimmerman, Nature 239 139 (1972)

2. J. A. Glaze, W. Simmons, F. Rainer, R. Boyd, C. Fetterman, E. Bliss and J. Murray, "CYCLOPS Single-Chain Prototype System", Laser Program Annual Report, UCRL-50021-74.

3. A. J. Campillo, S. L. Shapiro, and B. R. Suydam, Appl. Phys. Lett. 23 628 (1973)

4. V. I. Bespalov and V. I. Talanov, JETP Letters 3, 307 (1966)

5. E. S. Bliss, D. R. Speck, J. F. Holzrichter, J. H. Erkkila and A. J. Glass, Appl. Phys. Lett., 25 448 (1974)

6. E. S. Bliss, G. E. Sommargren, and H. J. Weaver. "Loss of Focusable Energy Due to Small-Scale Nonlinear Effects", IEEE/OSA CLEA Conference, May 28-30, 1975.

7. W. W. Simmons, S. Guch, Jr., F. Rainer, and J. E. Murray "A High Energy Spatial Filter for the Removal of Small Scale Beam Instabilities in High Power Solid State Lasers", IEEE/OSA CLEA Conference, May 28-30, 1975.

8. H. J. Weaver, E. Bliss and G. Sommargren, "Computerized Processing of Laser Diagnostic Data", Laser Program Annual Report UCRL-50021-74, p.p. 345-352.

9. J. B. Trenholme, Private Communication

10. J. A. Glaze, Lawrence Livermore Laboratory, Internal Memorandum, December 11, 1974.

11. A somewhat different, but equivalent, formulation is given by J. B. Trenholme in The Laser Program Annual Report, UCRL-50021-74, p.p. 84-88.

12. A. J. Campillo, R. A. Fisher, R. C. Hyer and S. L. Shapiro, Appl. Phys. Lett. 25, 408, (1974)

13. J. A. Glaze, D. R. Speck and J. T. Hunt, "Geometrical Theory of Nonlinear Phase Distortion of Intense Laser Beams", UCRL-76834 Preprint.

14. J. A. Glaze, W. W. Simmons and W. F. Hagen, "Quadratic Apodization: A Technique for Minimizing Intensity Induced Aberrations in High Power Lasers", Meeting of the Optical Society of America, October 21-24, 1975.

15. J. Hunt, P. Renard, J. Morris, and P. Thompson, "Propagation of Super-Gaussian and Quadratic Intensity Profiles - A Numerical Study", Laser Program Annual Report, UCRL-50021-74, p.p. 203-206. (There is an error in this report on page 203. The computer code used for the calculations in this report has erroneously been referred to as SLAB. The correct code designation is ZAX.)

16. J. T. Hunt, P. A. Renard and R. G. Nelson, "Focusing Properties of an Aberrated Laser Beam", UCRL-76328 Preprint

FIGURE CAPTIONS

1. CYCLOPS chain schematic. This chain is being used for laser development studies as well as target alignment and irradiation experiments.

2. CYCLOPS C-module. This amplifier has a clear aperture of 20 cm. When pumped with 280 kJ of bank energy it achieves a small signal gain of 6.5%/cm, corresponding to a net gain of 1.8. If liquid edge claddings are used for parasitic suppression the net gain rises to 2.

3. Photograph of the $f^{\#}/10$ spatial filter used between the B and C-amplifier stages on CYCLOPS. This filter has a clear aperture of 10 cm and employs a 300-μm diamond pinhole.

4. Simplified schematic of the CYCLOPS chain showing representative values for power and energy at each stage.

5. CYCLOPS laser chain - view from the C-amplifier output stage.

6. Beam photographs and densitometer scans showing the growth of shear-plate interference fringes spaced 2 mm apart on a pulse with peak intensity of 5 GW/cm^2.[5]

7. Effects of beam breakup on far-field energy distribution. Profile distortion indicates whole beam self-focusing; shrinking area illustrates small scale self-focusing.[6]

8. Temporal distortion due to small scale breakup.[6]

9. Near-field of C-amplifier output when CYCLOPS was operated without the B-stage spatial filter, at 270 J and 1 terawatt. The structure of the beam is revealed by the placement of four neutral density filters in front of the camera and near beam center.

10. Near field photographs of a structured beam before and after transmission through the B-stage spatial filter.

11. Percentage pulse power transmission of the B-stage spatial filter as a function of incident power for several pinhole diameters.[7]

12. Relative intensity/phase variation for the Airy disk, modified quadratic and super-gaussian beam shapes. (The phase retardation is proportional to the intensity through Equation 10.)

13. Relative angular variation of the rays in the near field. The angles have been normalized to the peak variation for that of the super-gaussian.[14]

14. Calculated intensity distribution of an aberrated beam at various receiving planes following the focusing lens.

15. Focal volume intensity distributions; a) diffraction limited plane wave with a super-gaussian intensity distribution and b) the same profile with 1.5 waves of whole beam distortion. The constant intensity contours are spaced 1 dB apart.(15,16)

16. Focal volume intensity distributions; a) diffraction limited plane wave with a modified-quadratic intensity distribution and b) the same profile with 1.5 waves of whole-beam distortion. The constant intensity contours are spaced 1 dB apart.(15,16)

CYCLOPS LASER SYSTEM

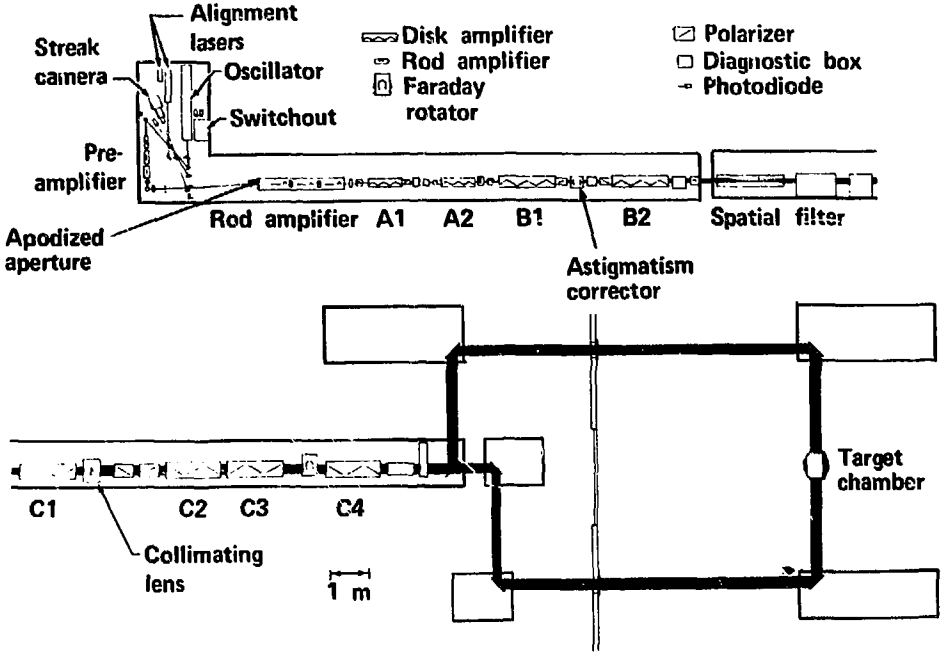

Fig. 1

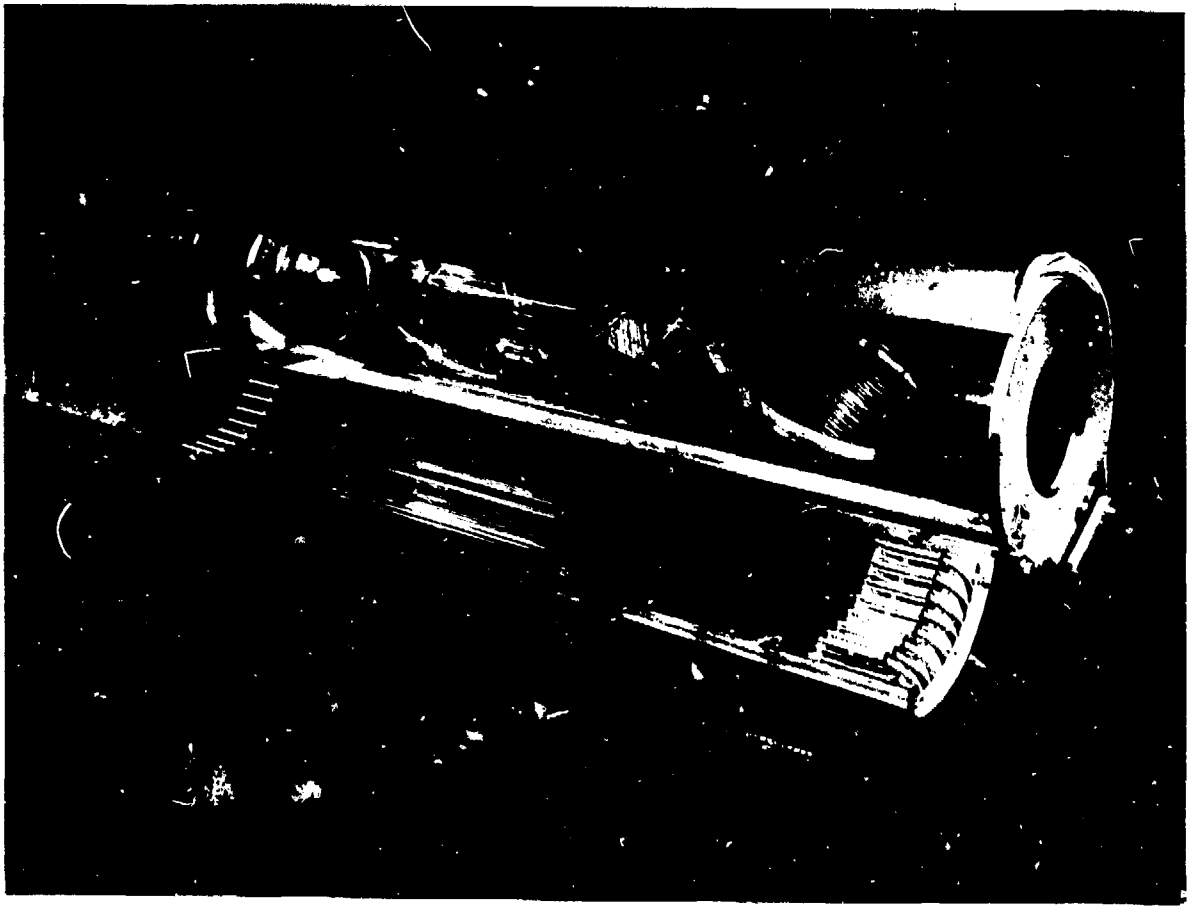

Fig. 2

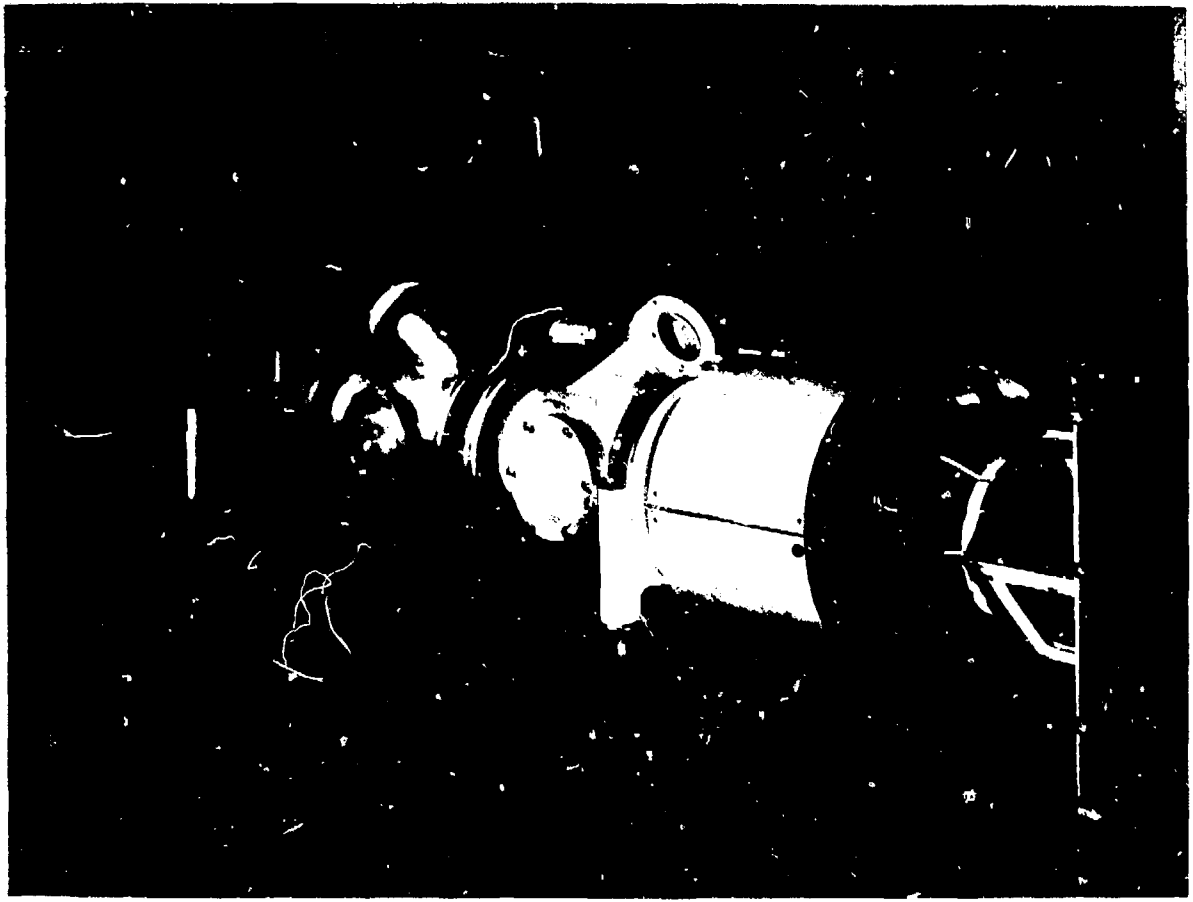

Fig. 3

CYCLOPS LASER SYSTEM 7-30-75

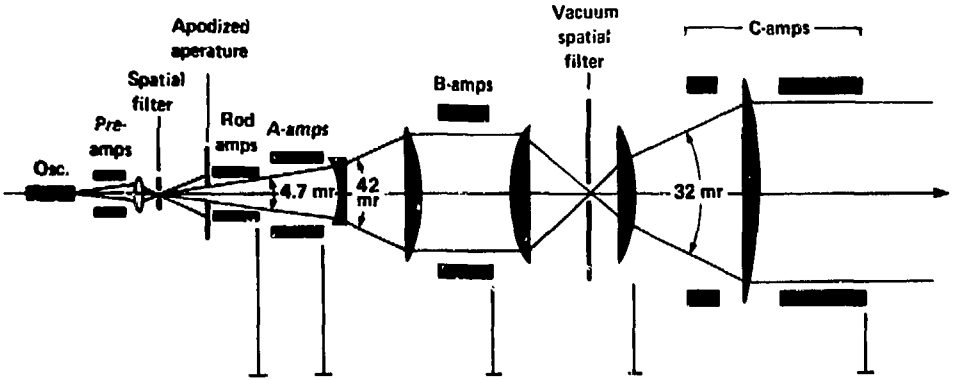

Energy	**0.15**	**1.0**	**23.9**	**16.2**	**97.8**
Power (GW)	1.7	11	260	176	1060
Bank energy (KJ)	**18**	**126**	**476**	–	**1152**
Aperture (mm)	**25**	**36**	**82**	–	**200**

Fig. 4

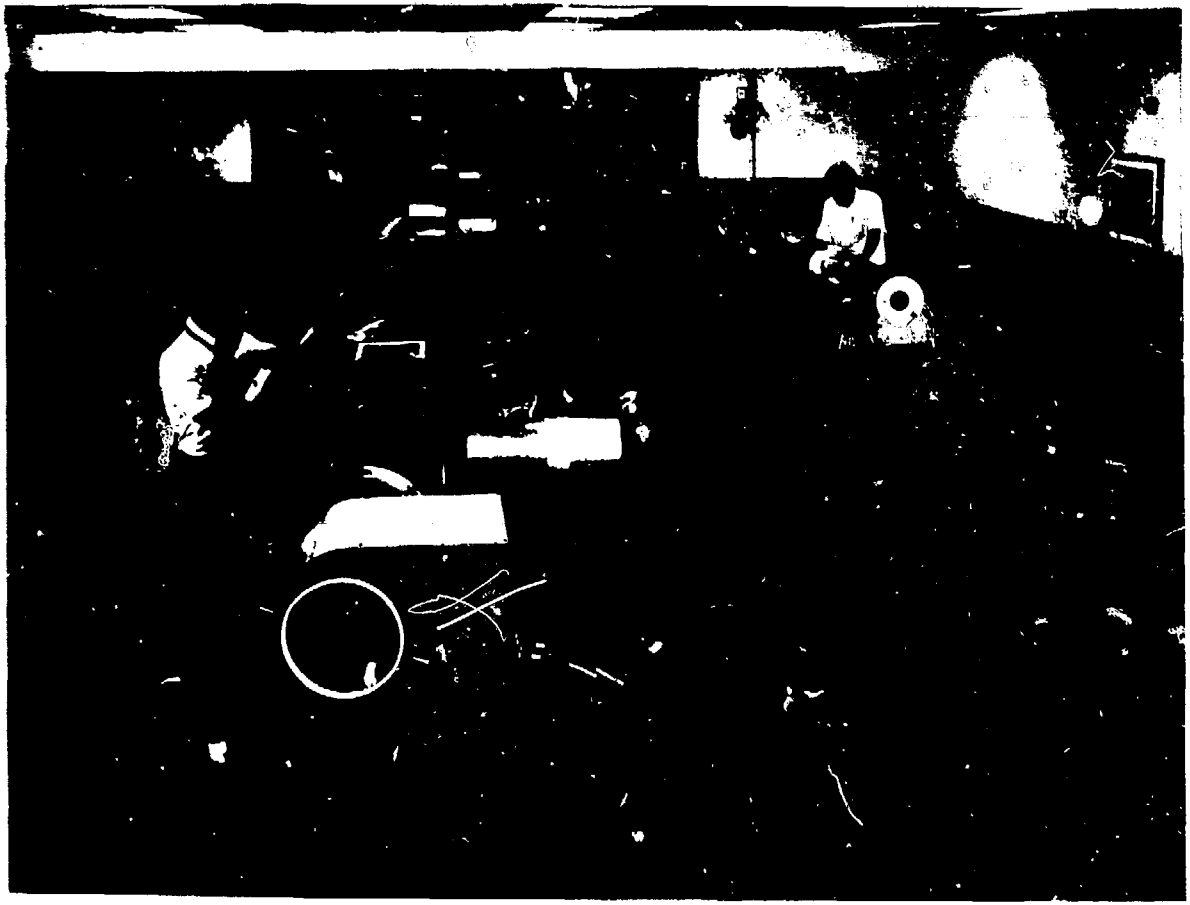

Fig. 5

MODULATION GROWTH IN A NONLINEAR MEDIUM

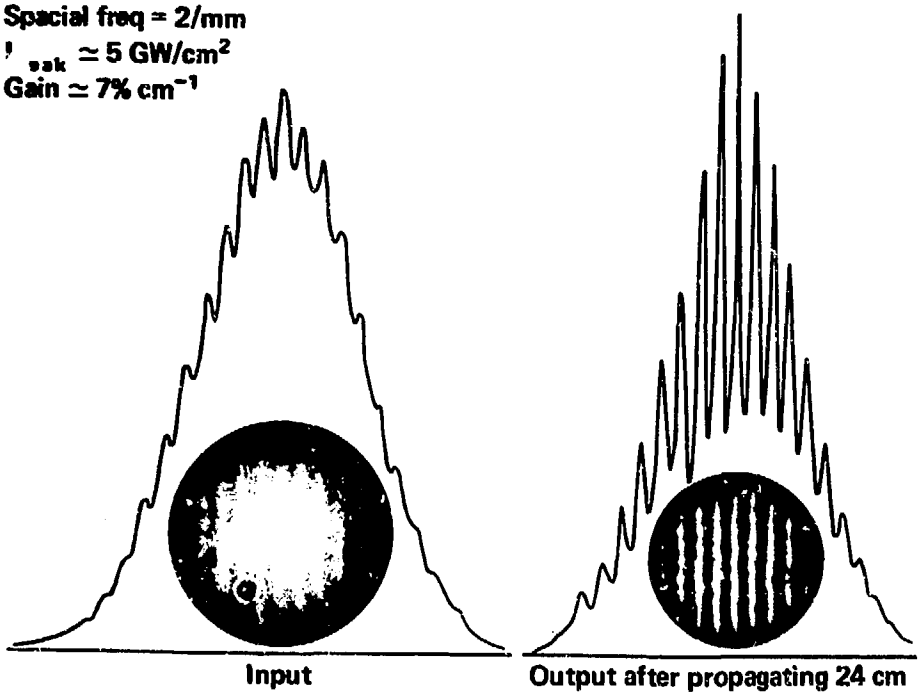

Fig. 6

QUALITATIVE; EXPERIMENTAL EFFECTS OF BEAM BREAKUP ON FAR-FIELD ENERGY DISTRIBUTION

Input beam; Gaussian with increasing B,

1. Profile distortion indicates whole beam self-focusing.
2. Shrinking area illustrates small-scale self focusing.

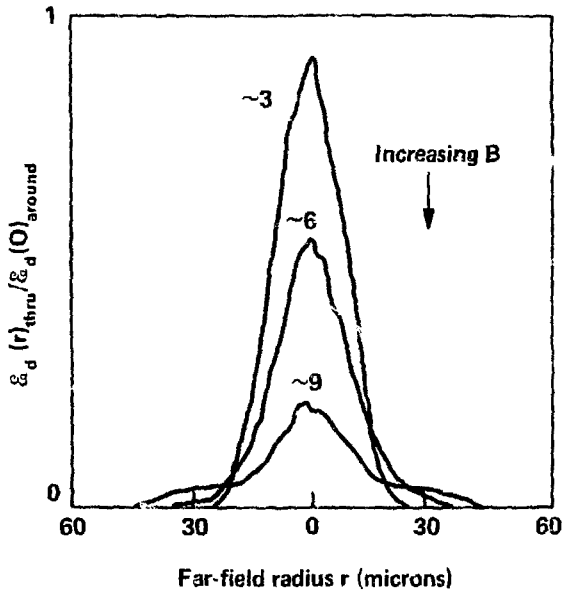

Fig. 7

TEMPORAL DISTORTION DUE TO SMALL-SCALE BEAM BREAKUP

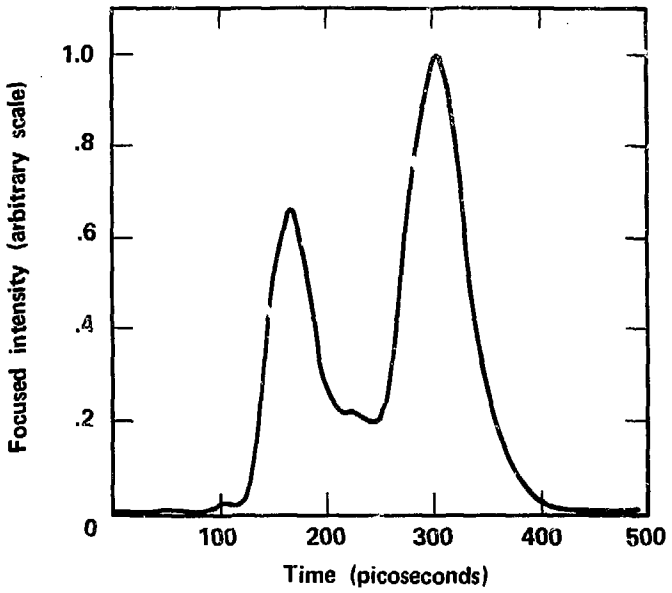

Fig. 8

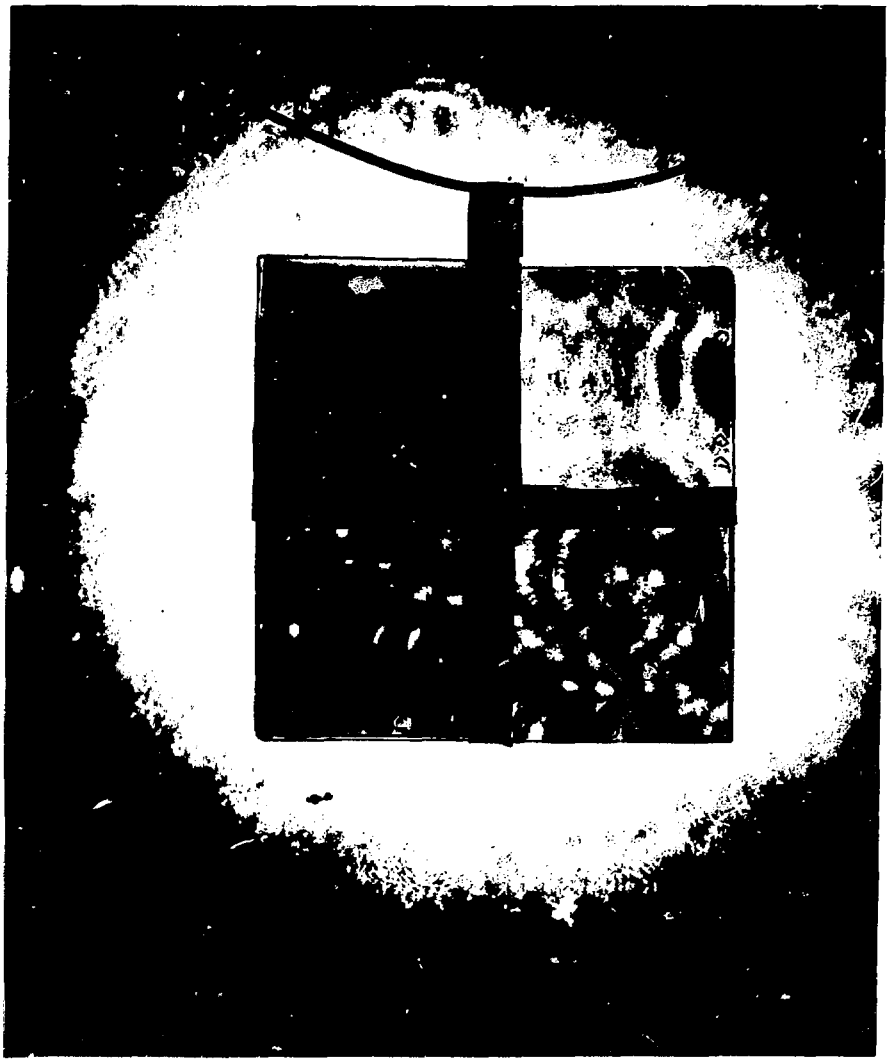

Fig. 9

CYCLOPS SPATIAL FILTER PERFORMANCE

Input

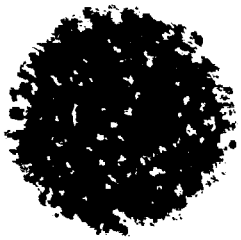

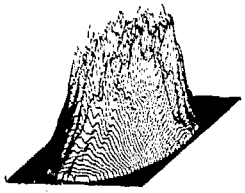

Output

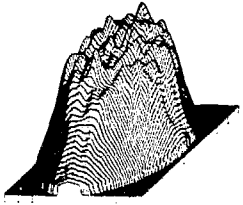

Near field | Contour plot | Energy density

Fig. 10

SPATIAL FILTER TRANSMISSION

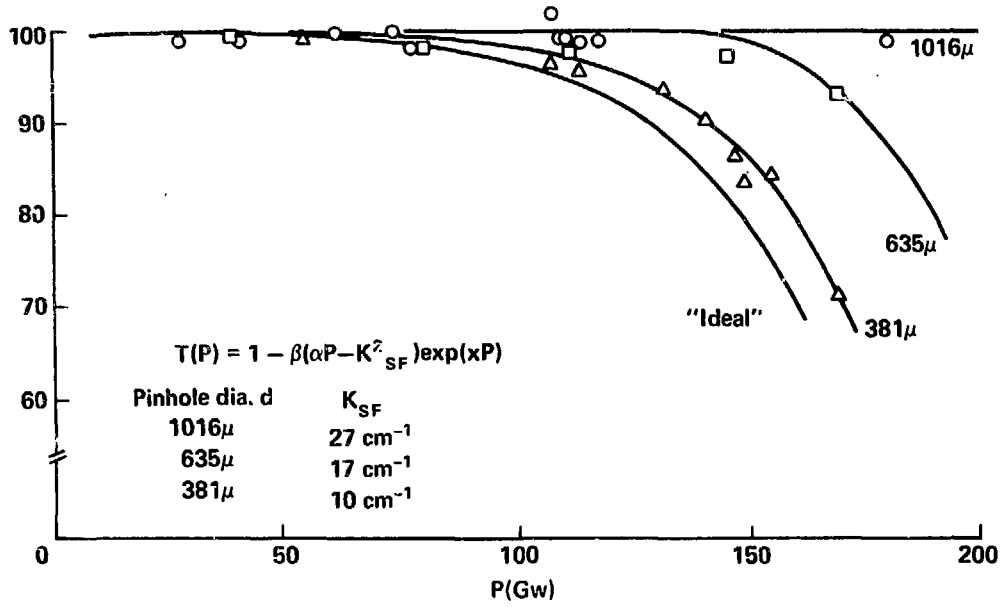

Fig. 11

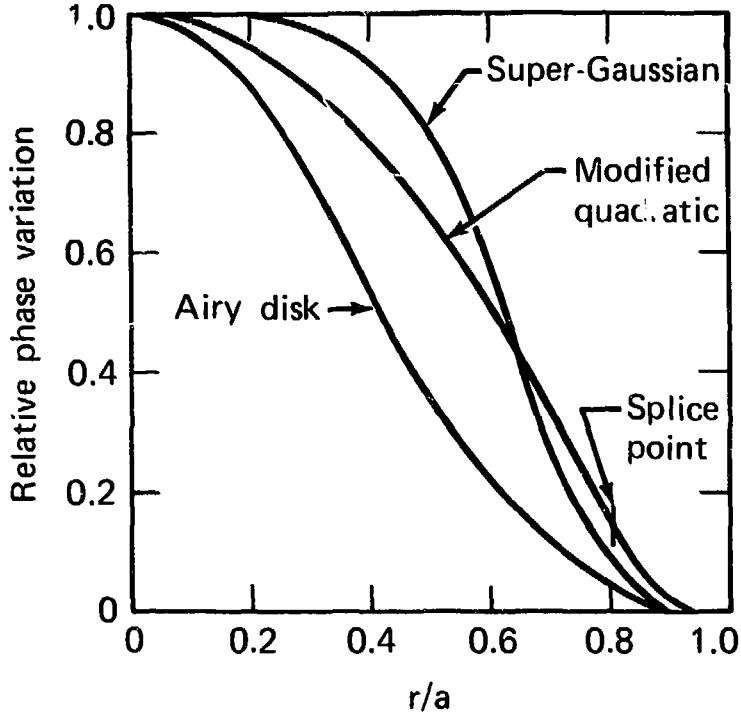
1.0
0.8
0.6
0.4
0.2
0
Relative phase variation
Super-Gaussian
Modified
quadratic
Airy disk
Splice
point
0
0.2
0.4
0.6
0.8
1.0
r/a

Fig. 12

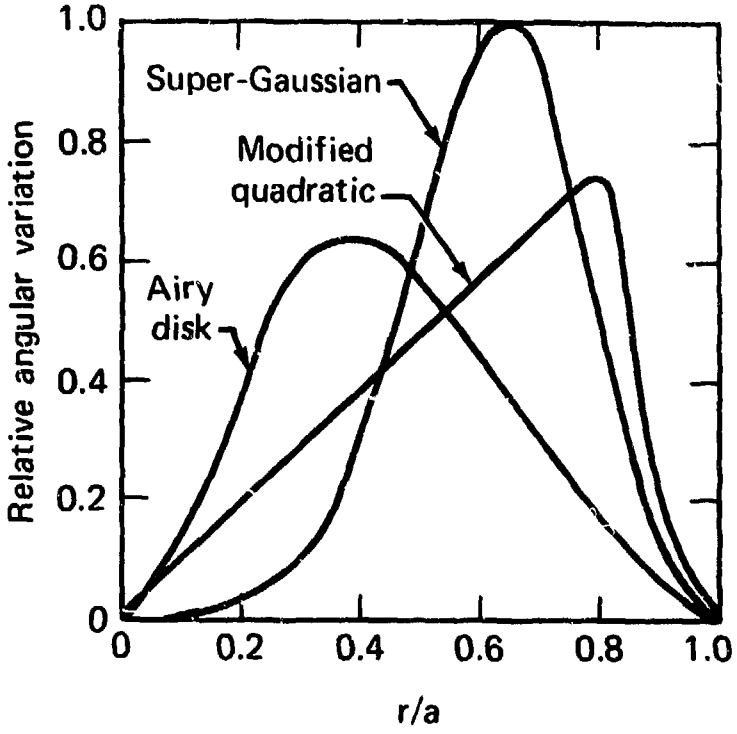
1.0
0.8
0.6
0.4
0.2
0
Relative angular variation
Super-Gaussian
Modified
quadratic
Airy
disk
0
0.2
0.4
0.6
0.8
1.0
r/a

Fig. 13

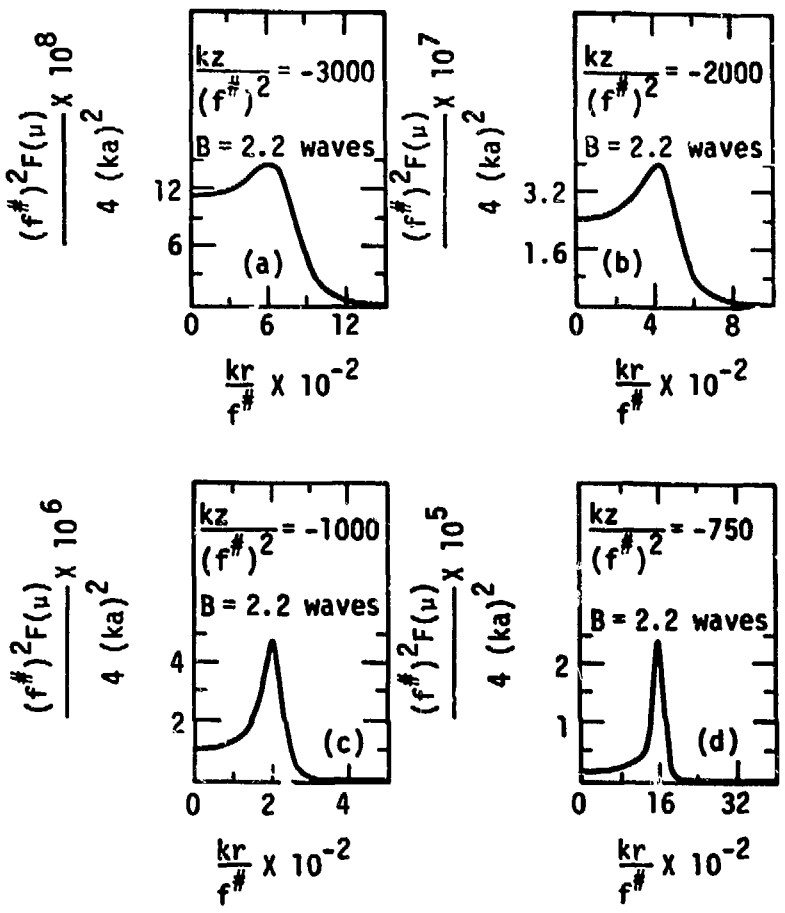
$\frac{(f^{\#})^2 F(\mu)}{4\,(ka)^2} \times 10^8$
$\frac{kz}{(f^{\#})^2} = -3000$
B = 2.2 waves
12
6
(a)
0
6
12
$\frac{kr}{f^{\#}} \times 10^{-2}$
$\frac{(f^{\#})^2 F(\mu)}{4\,(ka)^2} \times 10^7$
$\frac{kz}{(f^{\#})^2} = -2000$
B = 2.2 waves
3.2
1.6
(b)
0
4
8
$\frac{kr}{f^{\#}} \times 10^{-2}$
$\frac{(f^{\#})^2 F(\mu)}{4\,(ka)^2} \times 10^6$
$\frac{kz}{(f^{\#})^2} = -1000$
B = 2.2 waves
4
2
(c)
0
2
4
$\frac{kr}{f^{\#}} \times 10^{-2}$
$\frac{(f^{\#})^2 F(\mu)}{4\,(ka)^2} \times 10^5$
$\frac{kz}{(f^{\#})^2} = -750$
B = 2.2 waves
2
1
(d)
0
16
32
$\frac{kr}{f^{\#}} \times 10^{-2}$

Fig. 14

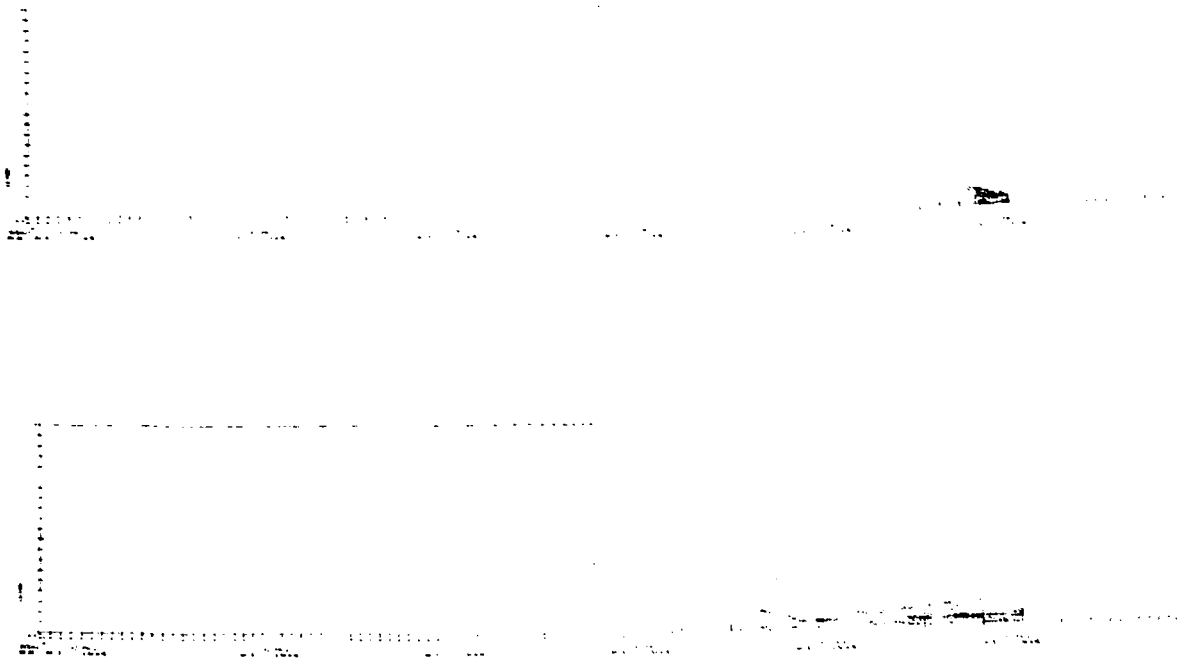

Fig. 15

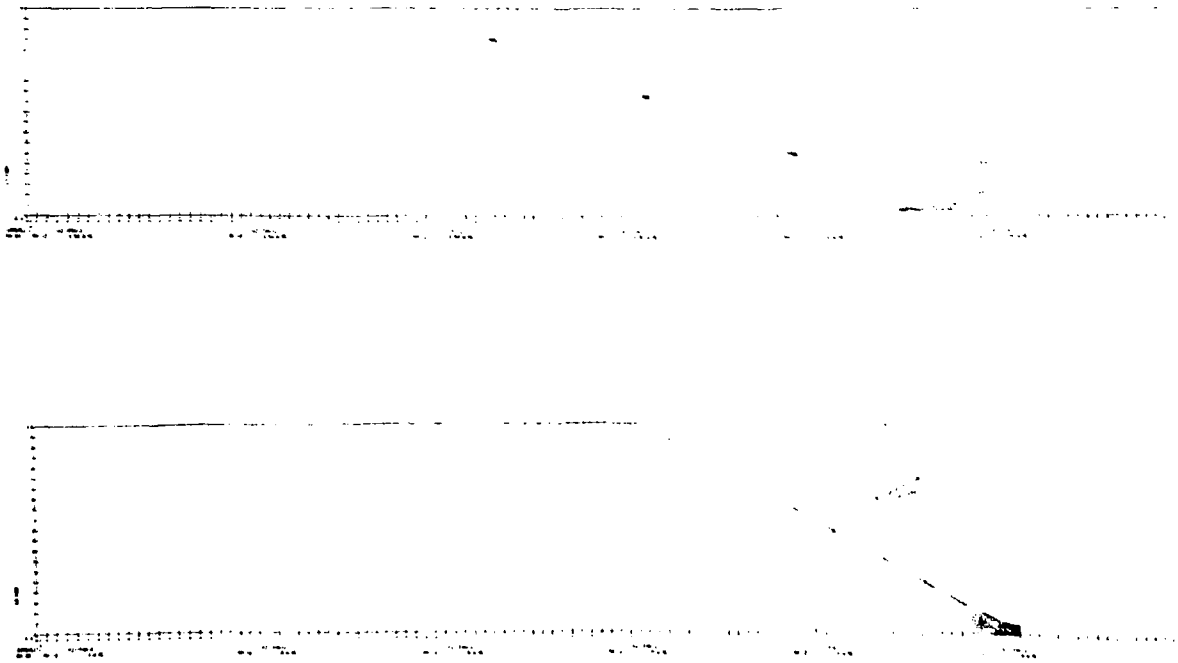

Fig. 16